Quantitative investigation of the validity conditions for the Beckmann-Kirchhoff scattering model

Helia Hooshmand*, Mingyu Liu, Richard Leach, Samanta Piano

Manufacturing Metrology Team, Faculty of Engineering, University of Nottingham, Nottingham, UK

Abstract. Approximate and rigorous methods are widely used to model light scattering from a surface. The boundary element method (BEM) is a rigorous model that accounts for polarisation and multiple scattering effects. BEM is suitable to model the scattered light from surfaces with complex geometries containing overhangs and re-entrant features. The Beckmann-Kirchhoff (BK) scattering model, which is an approximate model, can be used to predict the scattering behaviour of slowly-varying surfaces. Although the approximate BK model cannot be applied to complex surface geometries that give rise to multiple scattering effects, it has been used to model the scattered field due to its fast and simple implementation. While many of the approximate models are restricted to surface features with relatively small height variations (typically less than half the wavelength of the incident light), the BK model can predict light scattering from surfaces with large height variations, as long as the surfaces are "locally flat" with small curvatures. Thus far, attempts have been made to determine the validity conditions for the BK model. The primary validity condition is that the radius of curvature of any surface irregularity should be significantly greater than the wavelength of the light. However, to have the most accurate results for the BK model, quantifying the validity conditions is critical. This work aims to quantify the validity conditions of the BK model according to different surface specifications, e.g., slope angles and curvatures. For this purpose, the scattered fields from various sinusoidal and combinations of sinusoidal profiles are simulated using the BEM and the BK models and their differences are compared. The result shows that the BK model fails when there are high slope angles ($\gtrapprox$ 38°) and small radii of curvature ($\lessapprox$ 10 λ) within a sinusoidal profile. Moreover, it is shown that for a combination of sinusoidal profiles the BK model is valid for profiles with a high maximum slope angle value ($\gtrapprox$ 38°) if the average of positive slope angles is low ($\lessapprox$ 5°).

Keywords: light scattering, boundary element method, Beckmann-Kirchhoff, validity conditions, slope and curvature

*Helia Hooshmand, E-mail: helia.hooshmand@nottingham.ac.uk

1 Introduction

When a light beam illuminates an object with surface height variations of the order of or larger than the incident wavelength, the object scatters the light in various directions[1, 2], while in an optically flat object, specular reflection is dominant. For a certain object material and illumination condition (fixed incident angle, wavelength and polarisation), the scattering pattern depends on the surface topography of the object, and can be used to reveal topography information[2]. In conventional three-dimensional (3D) optical surface topography measurement instruments, e.g., coherence scanning interferometry (CSI), confocal microscopy and focus variation microscopy, the scattered field propagates through the optical instrument to form the raw images. The 3D surface topography is then obtained using an appropriate surface reconstruction method, e.g. envelope detection[3], frequency domain analysis[4] and the correlogram correlation method[5] in interference microscopy, contrast measurement methods in focus variation microscopy[6] and the use of fitting algorithms on the axial response in confocal microscopy[7]. As a result, modelling of light scattering is critical for any optical surface measurement system.

Scattering models can be categorised into two major groups: rigorous and approximate models. In rigorous models, such as the finite difference time domain (FDTD) method[8], finite element method (FEM)[9], rigorous coupled-wave analysis (RCWA)[10] and boundary element method (BEM)[11], numerical techniques are used to solve Maxwell’s equations. Rigorous models are complex and can be computationally intensive. However, to predict the scattered light from complex surface geometries containing overhangs and re-entrant features, or other types of geometries where multiple scattering occurs, only rigorous scattering models can be applied. All of the named rigorous models show different advantages regarding efficiency, accuracy and simplicity of modelling with respect to various applications[12, 13]. Thus far, various rigorous models have been adopted for confocal[14] and interference microscopy[12, 15, 16]. The BEM model solves linear partial differential equations only along the surface boundaries. BEM has been used in several applications including rigorous speckle simulation[17], modelling of the total electric field induced by transcranial magnetic simulation[18], development of acoustic holography algorithms for spatial transformation of sound fields radiated by irregularly shaped sources[19], development of a stable time domain method for the analysis of electromagnetic scattering and radiation problems[20], signal modelling in CSI for a vee-groove surface type[21] and a range of tilted blazed diffraction gratings[22], and in on-machine surface defect detection using light scattering and deep learning for sawtooth gratings[23].

Approximate scattering models make use of certain approximations to solve Maxwell's equations. Approximation models lead to different limitations in their ranges of validity which make them applicable only on weakly scattering media, surfaces with small height variations and/or slowly varying surfaces on the optical scale. Nevertheless, compared to rigorous methods, approximate models are straightforward to implement and computationally efficient. Furthermore, they provide direct insight into the scattering process and can often deliver an inverse solution to surface determination from the scattering data as they consider light scattering as a linear process[24]. One common approximate model is based on the small height approximation which can only be used on near planar surfaces[25]. The small height approximation relies on the assumption that the phase of the field at each point on the surface is directly proportional to the surface heights so that the surface can be replaced by a thin phase grating. The validity condition of the small height approximation is expressed by the depth of field, i.e. $h < \lambda/\mathrm{NA}^2$, where h is the surface height variation, λ is the illumination wavelength and NA is the numerical aperture of the objective lens[26]. The small height approximation along with a 2D representation of the propagating light field (referred to as the elementary Fourier optics model) has been used to model an interference microscope[26, 27]. The Rayleigh-Rice (also known as vector perturbation theory) can relate the surface power spectral density (PSD) of a slightly rough surface to the corresponding scattering pattern[28]. The perturbation approach is valid when the root-mean-square (RMS) of the surface height is small compared to the wavelength of the incident light. A widely used approximate model for weakly scattering medium is the first-order Born approximation[25] in which the total field (incident and scattered fields) can be replaced by the incident field. The main validity condition of the Born approximation is that the refractive index of the scattering medium should only differ slightly from unity.

Among the approximate models, the Beckmann-Kirchhoff (BK) solution (also known as the Kirchhoff approximation) is commonly applied to reduce the theoretical complexity of a rough surface scattering problem[2, 25]. The BK model is not restricted to small height surface variations and can predict light scattering from rough surfaces (i.e. surfaces with larger RMS heights than those used with perturbation methods). The BK model assumes that the local curvatures of the surface are small compared to the wavelength of the incident light, i.e., to fulfil the Kirchhoff approximation, the surface has to be locally flat. Therefore, the Kirchhoff approximation is appropriate for smooth surfaces without sharp edges.

The BK model has been used in various surface topography measurement applications including signal modelling[29, 30] and measurement and correction of the 3D transfer function with CSI[31], 3D image formation in focus variation microscopy[32], modelling the scattered light from rough surfaces[33, 34] and characterisation of laser powder bed fusion surfaces[35]. The validity of the BK model for surface scattering has been investigated in terms of the surface correlation length, angle of the incidence, RMS of heights, and the ratio of the width of the rectangular corrugations and the separation between adjacent corrugations to the incident wavelength[2, 36-38]. However, currently there are no well-established quantitative conditions under which the BK is valid (to the authors' knowledge).

In this paper, the scattered field from a range of sinusoidal profiles (using a range of different pitch and height values) and various combinations of sinusoidal profiles (using combinations of a different number of sinusoidal profiles with different height values) - with different radii of curvature (ROC) and slope angles (SA) - has been simulated using the 2D BK model and the 2D BEM model. The validity conditions of the BK model depend on the radius of curvature and the local angle of incidence[2]. In this work, we investigated the validity conditions of the BK model based on the values of the minimum ROC and maximum SA. Since the minimum ROC appears in the minimum of the sinusoidal profile, the local incident angle and the incident angle are the same. The angular distribution of the scattering patterns of each profile obtained by the BK model is compared to those from the BEM model using the RMS of the difference of normalised scattered fields (NSFs). To achieve a clear understanding of the validity conditions of the BK model, variation of the RMS of the difference of the NSFs has been investigated in terms of the change in the minimum ROC and maximum SA of the sinusoidal profiles, and the maximum SA and average of positive SAs of a combination of the sinusoidal profiles. Some primary results have been presented previously[39]. It is shown that the presence of the low ROC (compared to the wavelength of the incident light) and high slope angle within a sinusoidal profile result in multiple scattering and causes the BK model to fail. However, the BK model is able to predict the scattered field from a combination of sinusoidal profiles with a high maximum SA if the average of positive SAs within the profile is low.

2 Rigorous and approximate scattering models

2.1 Modelling of the scattered field using the rigorous BEM model

The rigorous BEM model used in this work is based on the work by Simonsen[40], while the theory was developed earlier by Maradudin et al.[41]. The BEM model finds the total field and its normal derivative along the surface by taking advantage of the Ewald-Oseen extinction theorem[42] and solves the subsequent set of inhomogeneous integral equations through conversion to matrix equations by appropriate spatial discretisation of the integrals. This approach provides an exact solution and accounts for the multiple scattering and polarisation effects; therefore, this model is promising for arbitrarily complex surfaces. The 2D version of the BEM algorithm is restricted to prismatic surfaces that can be fully described in the plane of incidence, assuming the surface is infinitely extended along the third dimension, perpendicular to the incidence plane. The scattering outside the incidence plane is considered negligible for prismatic surfaces, and this feature means that the 2D BEM model is able to simulate the scattered field without significant loss of accuracy. According to the integral theorem of Helmholtz and Kirchhoff[25], the scattered field $E_s(r)$ from any surface can be expressed from the values of the total field $E(r')$ and its normal derivative, $\partial E(r')/\partial n'$ on the surface s

$$E_s(r) = \iint_s \left[G(r-r') \frac{\partial E(r')}{\partial n'} - E(r') \frac{\partial G(r-r')}{\partial n'} \right] ds, \tag{1}$$

where $G(r-r')$ is the Green's function of the Helmholtz operator and $\partial/\partial n'$ denotes differentiation along the outward normal to the surface. In the BEM model, the total field and its normal derivatives at given points on the surface are calculated globally, taking into account the contribution of all neighbouring points. As a result, the BEM model is able to address multiple scattering effects. Accordingly, the scattering surface is divided into several discrete points, and for each point, the Kirchhoff surface integral and the boundary conditions are applied. Values for the field and its normal derivative at each point can be obtained by solving the coupled matrix equations[40]. Eventually, the BEM finds the surface "source" fields, from which the far-field scattering at any point can be calculated.

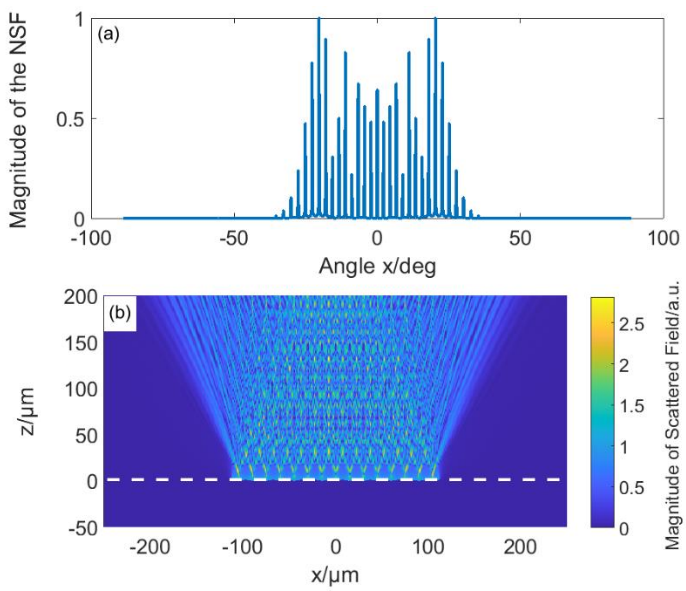

Figure 1. 2D BEM scattered field from a sinusoidal profile with 15 µm pitch, 1 µm height and 225 µm length (a) angular distribution of the magnitude of the NSF (unitless), (b) magnitude of the scattered field in the incidence plane obtained by the BEM model.

As an example, the BEM model was applied to a 2D sinusoidal profile with a 15 µm pitch, 1 µm peak-to-valley distance (height) and 225 µm length (includes fifteen cycles). The angular distribution of the magnitude of the NSF and its 2D visualisation in the incidence plane obtained by the 2D BEM are shown in Figure 1 (a) and (b), respectively. Normalisation is done by dividing the amplitude at each angle by the maximum value of the amplitude over the angular range. The incident illumination was chosen to be a transverse electric field (TE polarisation) with a monochromatic plane-wave ($\lambda = 0.58$ μm) normal to the surface profile. The far-field scattered field was calculated over 777 observation angles sampled from -88° to 88° to cover the widest possible range of the angular distribution.

2.2 Modelling of the scattered field using the approximate BK model

Consider a monochromatic plane-wave $E_i(\mathbf{r}) = \exp(2\pi i \mathbf{k_i}.\mathbf{r})$ propagating with the 3D wave vector $\mathbf{k_i}$ illuminating a 3D scattering object. The Kirchhoff boundary conditions approximate the total field (E) and its normal derivative at a surface point $\mathbf{r_s}$ and can be written as[2]

$$E(\mathbf{r_s}) = (1+R)E_i(\mathbf{r_s}), \tag{2}$$

$$\frac{\partial E(\mathbf{r_s})}{\partial n} = 2\pi \mathbf{k_i}.\hat{\mathbf{n}}(1-R)E_i(\mathbf{r_s}), \tag{3}$$

where $\hat{\mathbf{n}}$ is the normal to the surface at $\mathbf{r_s}$, and R is the Fresnel amplitude reflection coefficient (assumed to be constant over the range of desired scattering angles).

Substituting Eqs. (2) and (3), and the free-space Green's function $G = \exp(2\pi i k_0 |\mathbf{r}|)/4\pi|\mathbf{r}|$ into the Kirchhoff surface integral of Eq. (1), the far-field scattered field can be written as[29]

$$\tilde{E}_s(\mathbf{K}+\mathbf{k_i}) = -\frac{1}{2k_0}\delta\left(|\mathbf{K}+\mathbf{k_i}| - k_0\right)\left[\frac{|\mathbf{K}|^2}{\mathbf{K.z}}\right]\iiint R\delta\left[r_z - Z_s(r_x, r_y)\right]\exp(-2\pi i \mathbf{K.r})d^3r, \tag{4}$$

where $\mathbf{K} = \mathbf{k_s} - \mathbf{k_i}$ and $\mathbf{k_s}$ is the scattering wave vector (for elastic scattering $|\mathbf{k}_s| = |\mathbf{k}_i| = k_0 = 1/\lambda$). In Eq. (4), the term $4\pi i R\delta\left[r_z - Z_s(r_x, r_y)\right]$ is referred to as the "foil model" of the surface[29]. Based on the foil model, the object can be replaced by a 1D Dirac delta function representing the value of the reflection coefficient at each point on the surface. Note that Eq. (4) is valid only when integrating over a finite area in the xy plane ($R \neq 0$).

The scattered field over the whole surface is obtained by a 3D surface transfer function (STF) given by

$$\tilde{G}(\mathbf{K}+\mathbf{k_i}) = \frac{i}{4\pi k_0}\delta\left(\left|\mathbf{K}+\mathbf{k_i}\right| - k_0\right). \tag{5}$$

In other words, all possible scattered wave vectors $\mathbf{k}_s$ due to the incident wave vector $\mathbf{k_i}$ construct a spherical shell (Ewald sphere) in the **K** space, which is centered at $-\mathbf{k_i}$ and has a radius k_0 [43].

Using the definition of the STF, Eq. (4) can be re-written as

$$\tilde{E}_s(\mathbf{K}+\mathbf{k_i}) = \left[\frac{\left|\mathbf{K}\right|^2}{2\mathbf{K.z}}\right]\tilde{G}(\mathbf{K}+\mathbf{k_i})\tilde{F}_K(\mathbf{K}), \tag{6}$$

where $\tilde{F}_K(\mathbf{K}) = 4\pi i \iiint R\delta\left[r_z - Z_s(r_x, r_y)\right]\exp(-2\pi i\mathbf{K.r})d^3r$ is the Fourier transform of the foil model of the object. Eq. (6) shows that in the BK model, the scattering is considered as a linear filter (defined by the STF) applied to the foil model of the surface.

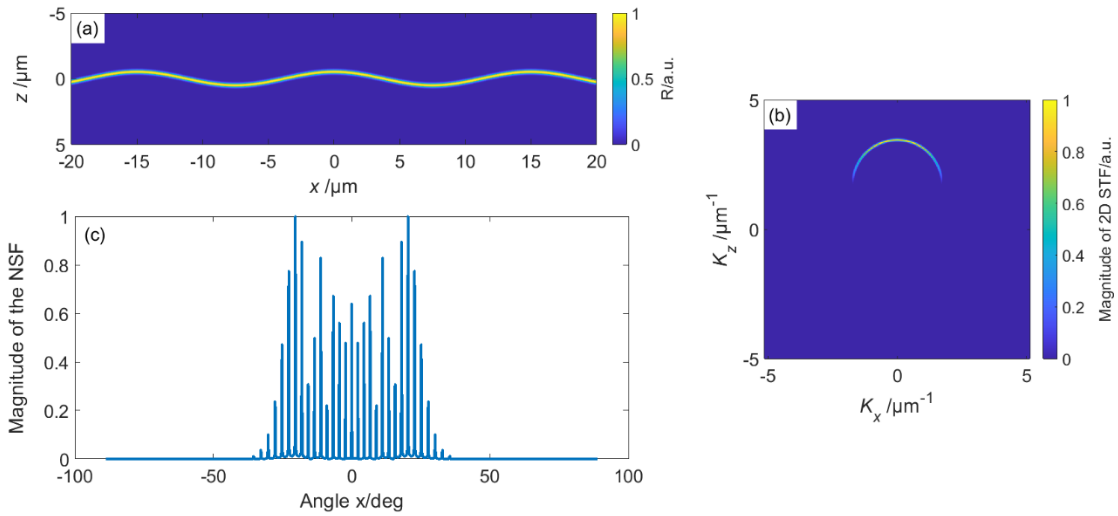

Figure 2. 2D BK scattered field from a sinusoidal profile with 15 µm pitch, 1 µm height and 225 µm length (a) 2D foil model of the surface (generated over the same length, with the display window being trimmed for better visualisation), (b) 2D STF and (c) angular distribution of the magnitude of the NSF (unitless).

As shown in Eqs. (2) – (6), the BK model can be applied to 3D surfaces to find the scattered field in 3D. However, we used the 2D version of Eqs. (6) to compare the results with those obtained by the BEM model.

As an example, the BK model was applied to a 2D sinusoidal profile with a 15 µm pitch, 1 µm peak-to-valley distance (height) and 225 µm length (includes fifteen cycles). Figure 2 (a) illustrates the 2D foil model of the sinusoidal profile. If the Fourier transform of the foil model of the surface is to be obtained numerically by the discrete Fourier transform of the object function, the delta function should be defined as a limit of a Gaussian function. The standard deviation of the Gaussian function should be chosen to be consistent with the sampling conditions of the discrete Fourier transform calculation to avoid aliasing problems[44]. In Figure 2(b), the 2D STF with a monochromatic plane wave ($\lambda = 0.58$ µm) that is normal to the surface profile is shown. The scattered far-field was calculated over 777 observation angles sampled from -88° to 88°. The angular distribution of the magnitude of the NSF obtained by the 2D BK model is shown in Figure 2 (c).

3 Method

In order to find the validity condition of the approximate BK model, experiments involving quantitative comparisons between the scattered fields obtained by the BK and the BEM models were designed. The incident illumination was chosen to be an unpolarised monochromatic plane-wave (λ = 0.58 μm) normal to the surface of a perfect conductor. A range of sinusoidal profiles with various minimum ROCs and maximum SAs and various combinations of sinusoidal profiles with different maximum SA and average of positive SAs values were investigated. In each case, the RMS of the differences between the NSF obtained by the BK and the BEM models was calculated. RMS is calculated by the square root of the average over all angles of the squares of the amplitude differences between the BK and the BEM models. Both models compute the scattered far-fields over the same angular distribution. The range of angles is determined by the sampling resolution of the profile. To obtain accurate far-field scattering results, the surface is sampled equidistantly, with the sampling distance set to be smaller than $\lambda/5$. In this work, decreasing the sampling distance lower than $\lambda/5$ does not change the peak value of the scattered field. Therefore, to avoid computational complexity the sampling distance is set to $\lambda/5$. The range of the angular distribution is fixed between -88° to 88°. As the profile is considered to be continuously repeated in the BK model (as a property of the FFT algorithm), in order to reasonably compare scattered fields from a sinusoidal profile for the BK and the BEM models, the length of the profile is set to include at least ten cycles. In the BEM model, the square values of the magnitude of the scattered field regarding the TE and TM polarisations have been added together. The root square of the result presents the magnitude of the scattered field of unpolarised light. For the BK model, the Fresnel reflection coefficient equals 1 for both polarisations. To illustrate the comparison, the BK and the BEM models have been applied to a sinusoidal profile with a minimum ROC of 0.5 μm and maximum SA of 38°. Figure 3 shows the angular distribution of the magnitude of the NSFs obtained by the BEM and BK models.

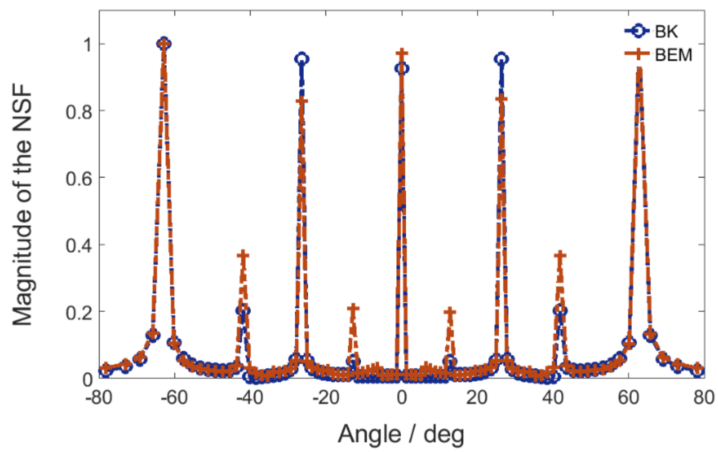

Figure 3. Angular distribution of the magnitude of the NSF obtained by the BK and the BEM models for a sinusoidal profile with a minimum ROC of 0.5 μm and maximum SA of 38°.

4 Results and discussion

In this section, the BEM and the BK model are applied to a range of sinusoidal profiles and various combinations of sinusoidal profiles. Profiles are simulated in terms of different lengths, pitches, heights, minimum ROCs, maximum SAs and average of positive SAs. The scattered fields obtained by the BEM and the BK models are compared for each profile.

4.1 Comparison in terms of pitch and height values for profiles with lengths of ten times the pitch values

Variations of the RMS of the difference of the normalised scattered far-fields obtained by the BEM and the BK models from various sinusoidal profiles from Table 1 are shown in Figure 4. As shown in Table 1, a wide range of variations in ROC and SA (maximum SA between 2° and 72° and minimum ROC between 1 μm and 507 μm) were considered for comparison. Sinusoidal profiles are simulated by defining the height and pitch values as the input parameters. Enlarging the height of a sinusoidal profile with a certain pitch results in higher SA and lower ROC values. On the other hand, increasing the pitch value for a fixed height results in lower SA and higher ROC within a profile. To meet the comparison criteria for the BK model, the length of the profile was equal to ten times the pitch value for each case. The general trend in Figure 4 shows that increasing the height and decreasing the pitch values causes the RMS of the differences of the NSFs to increase. Increasing the pitch causes an insignificant rise in the RMS value (less than 0.02) particularly for low-height profiles (less than 10 μm). The increment occurs due to a large number of points for high-length profiles.

Table 1. Specifications of the sinusoidal profiles (in terms of pitch and height values) used to compare the far-field scattering fields obtained by the rigorous BEM and approximate BK models (via the RMS of the differences of the NSFs). Min ROCs are in micrometres.

Height/μm \ Pitch/μm	1	5	10	15	20
20	Min ROC: 20	Min ROC: 4	Min ROC: 2	Min ROC: 1	Min ROC: 1

	Max SA : 9°	Max SA: 38°	Max SA: 57°	Max SA: 67°	Max SA: 72°
30	Min ROC: 45 Max SA: 6°	Min ROC: 9 Max. SA: 27°	Min ROC: 4 Max SA: 46°	Min ROC: 3 Max SA: 57°	Min ROC: 2 Max SA: 64°
40	Min ROC: 81 Max SA: 4°	Min ROC: 16 Max SA: 21°	Min ROC: 8 Max SA: 38°	Min ROC: 5 Max SA: 50°	Min ROC: 4 Max SA: 57°
50	Min ROC: 157 Max SA: 4°	Min ROC: 25 Max SA: 17°	Min ROC: 13 Max SA: 32°	Min ROC: 8 Max SA: 43°	Min ROC: 6 Max SA: 51°
60	Min ROC: 182 Max SA: 3°	Min ROC: 36 Max SA: 15°	Min. ROC: 18 Max SA: 28°	Min ROC: 12 Max SA: 38°	Min ROC: 9 Max SA: 46°
70	Min ROC: 248 Max SA: 2°	Min ROC: 50 Max SA: 13°	Min ROC: 25 Max SA: 24°	Min ROC: 17 Max SA: 34°	Min ROC: 12 Max SA: 42°
80	Min ROC: 324 Max SA: 2°	Min ROC: 65 Max SA: 11°	Min ROC: 32 Max SA: 21°	Min ROC: 22 Max SA: 30°	Min ROC: 6 Max SA: 38°
90	Min ROC: 410 Max SA: 2°	Min ROC: 82 Max SA: 10°	Min ROC: 41 Max SA: 19°	Min ROC: 27 Max SA: 28°	Min ROC: 20 Max SA: 35°
100	Min ROC: 507 Max SA: 2°	Min ROC: 101 Max SA: 9°	Min ROC: 51 Max SA: 17°	Min ROC: 34 Max SA: 25°	Min ROC: 25 Max SA: 32°

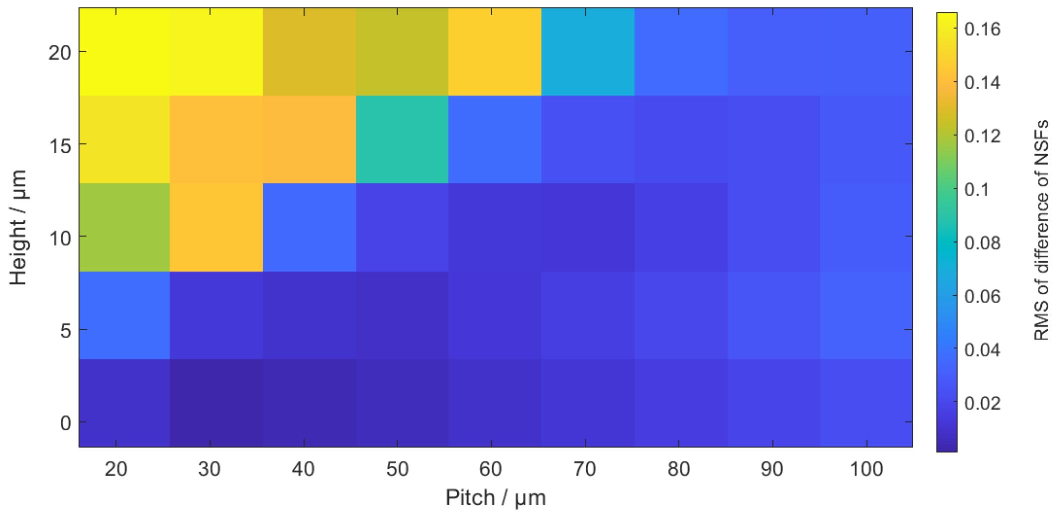

Figure 4. Variations of the RMS of the differences of the NSFs obtained by the BEM and the BK models for the sinusoidal profiles of Table 1 versus changes in the pitch and height values of the profiles. The length of the profiles was considered ten times the pitch value for each case.

4.2 Comparison in terms of pitch and height values for profiles with a fixed length of 600-μm

If the length of a profile changes, the angular resolution of the calculated far-field scattering varies. To compare the BK and the BEM scattering fields for a set of sinusoidal profiles with a fixed angular resolution, the profiles shown in Table 2 were analysed.

Figure 4 illustrates the variations of the RMS of the differences of the NSFs obtained by the BEM and the BK models for the sinusoidal profiles from Table 2 against changes in the pitch and height values of the profiles. The length of the profiles was 600 μm, so each profile includes at least ten cycles. The far-field scattering was sampled over 2069 observation angles from -88° to 88°. The results are in agreement with those obtained in Figure 4.

Table 2. Specification of the sinusoidal profiles (in terms of pitch and height values) used to compare the far-field scattering fields obtained by the rigorous BEM and approximate BK models (via the RMS of the differences of the NSFs). Min ROCs are in micrometres.

Height/μm **Pitch/μm**	**2**	**4**	**6**	**8**	**10**
20	Min ROC: 10 Max SA: 17°	Min ROC: 5 Max SA: 32°	Min ROC: 3 Max SA: 43°	Min ROC: 2 Max SA: 51°	Min ROC: 2 Max SA: 57°
30	Min ROC: 23 Max SA: 12°	Min ROC: 11 Max SA: 23°	Min ROC: 8 Max SA: 32°	Min ROC: 6 Max SA: 40°	Min ROC: 4 Max SA: 46°
40	Min ROC: 40 Max SA: 9°	Min ROC: 20 Max SA: 17°	Min ROC: 13 Max SA: 25°	Min ROC: 10 Max SA: 32°	Min ROC: 8 Max SA: 38°
50	Min ROC: 63 Max SA: 7°	Min ROC: 32 Max SA: 14°	Min ROC: 21 Max SA: 21°	Min ROC: 16 Max SA: 27°	Min ROC: 13 Max SA: 32°
60	Min ROC: 91 Max SA: 6°	Min ROC: 46 Max SA: 12°	Min ROC: 30 Max SA: 17°	Min ROC: 23 Max SA: 23°	Min ROC: 18 Max SA: 28°

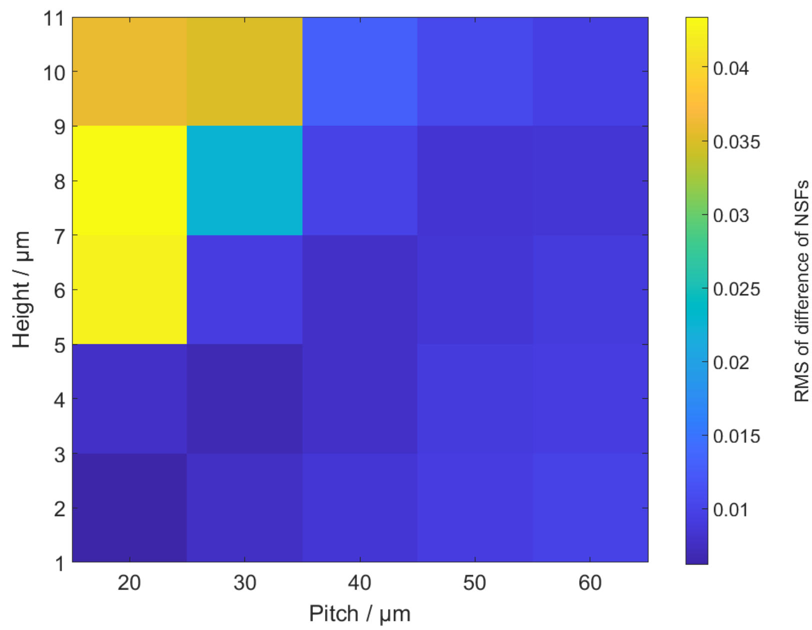

Figure 5. Variations of the RMS of the differences of the NSFs obtained by the BEM and the BK models for the sinusoidal profiles of Table 2 versus changes in the pitch and height values of the profiles. The length of the profiles was 600 µm (including at least ten cycles for each case).

4.3 Comparison in terms of minimum ROC and maximum SA for profiles with lengths of ten times the pitch values

Figure 6 shows the variations of the RMS of the differences of the NSFs obtained by the BEM and the BK models for the sinusoidal profiles shown in Table 3 against changes in the minimum ROC and maximum SA within the profile. The length of the profiles was considered to be ten times the pitch value for each case. As shown in Figure 6, increasing the maximum SA and decreasing the minimum ROC of the profile causes the RMS of the differences of the NSFs to increase. For the profile with a 5 µm minimum ROC ($>> \lambda$), increasing the maximum SA moderately changes the RMS of difference up to 58°. For a profile with a 0.5 µm minimum ROC ($\approx \lambda$) increasing the maximum SA ($\gtrsim$ 38°) results in a significant change in the RMS of the difference, indicating that there is a considerable difference between the BK and the BEM scattered fields.

In general, for the approximate BK model to predict the scattered field from a sinusoidal profile accurately, it is required that the minimum ROC of the profile is significantly greater than the incident wavelength ($\gtrsim 10\ \lambda$). Furthermore, even for profiles with a large minimum ROC (5 µm), the BK model is in good agreement with the BEM model if the maximum slope angle of the profile does not exceed a certain value ($\lesssim$ 38°). For SAs approximately higher than 38°, the BK model fails due to the effects of multiple scattering.

Table 3. Specifications of the sinusoidal profiles (in terms of minimum ROC and maximum SA values) used to compare the scattering far-fields obtained by the rigorous BEM and approximate BK models (via the RMS of the differences of the NSFs). Pitches and heights are in micrometres.

Max SA /deg \ **Min ROC /µm**	**0.5**	**2.5**	**5**
18	Pitch: 1 Height: 0.10	Pitch: 5 Height: 0.50	Pitch: 10 Height: 1
28	Pitch: 1.6 Height: 0.27	Pitch: 8.1 Height: 1.35	Pitch: 16.2 Height: 2.70
38	Pitch: 2.6 Height: 0.65	Pitch: 12 Height: 3	Pitch: 24 Height: 6
48	Pitch: 3.4 Height: 1.19	Pitch: 18 Height: 6.42	Pitch: 36 Height: 12.70
58	Pitch: 5.1 Height: 2.55	Pitch: 25 Height: 12.50	Pitch: 50 Height: 25
72	Pitch: 10 Height: 10	Pitch: 50 Height: 50	-

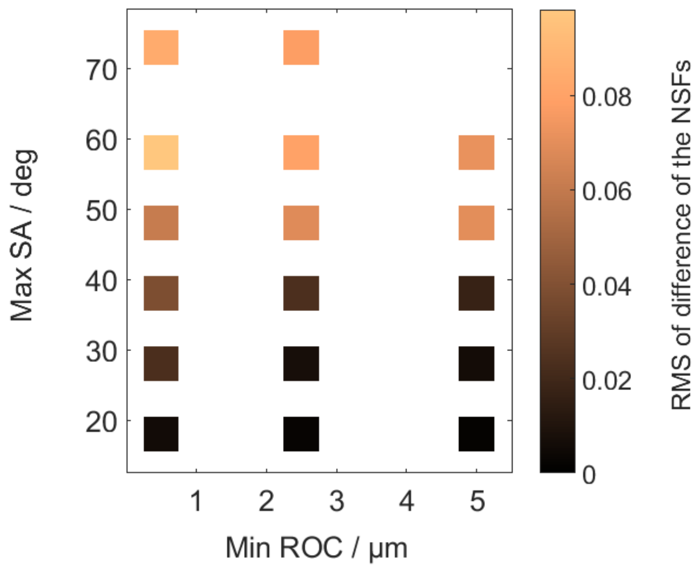

Figure 6. Variations of the RMS of the difference of the NSFs obtained by the BEM and the BK models regarding the sinusoidal profiles of Table 3 versus changes of the minimum ROC and maximum SA values of the profile. The length of the profiles was considered 10 times the pitch value for each case.

4.4 Comparison in terms of maximum SA and average of positive SAs for combinations of profiles with lengths of ten times a fixed pitch value

Figure 7 shows the variations of the RMS of the differences of the NSFs obtained by the BEM and the BK models for various combinations of sinusoidal profiles shown in Table 4 against changes in the average of positive SAs and maximum SA within the profile. The length of the profiles was considered to be ten times the fixed pitch value of 42 µm. As shown in Figure 7, increasing the maximum SA and the average of the positive SAs of the profile causes the RMS of the differences of the NSFs to increase. In line with the results obtained for single sinusoidal profiles, increasing the maximum SA of a profile results in a higher value for the RMS of the differences of the NSFs. However, for a combination of sinusoidal profiles changes in the RMS of the differences of the

NSFs against maximum SA for profiles with a lower average of positive SAs ($\lesssim$ 10°) are insignificant. As shown in Table 4, increasing the number of sinusoidal profiles in a series causes the average value of the positive SAs within a profile to decrease. Results show that even for a combination of sinusoidal profiles with a high maximum SA value ($\gtrsim$ 38°), the BK model is able to predict the scattered field accurately if the average of the positive SAs is low ($\lesssim$ 5°). Furthermore, the results indicate the independence of the validity of the BK model to the minimum ROC within a combination of sinusoidal profiles. However, for the approximate BK model to deliver accurate results in a combination of sinusoidal profiles, it is required that the average of the ROC of the profile is significantly greater than the incident wavelength ($\gtrsim$ 10 λ).

Table 4. Specifications of various combinations of sinusoidal profiles (in terms of the average of positive SAs and maximum SA values) used to compare the scattering far-fields obtained by the rigorous BEM and approximate BK models (via the RMS of the differences of the NSFs). Heights are in micrometres and the pitch value is fixed at 42 μm for all profiles.

Average of positive SAs /deg / **Max SA /deg**	**1.5**	**4.5**	**8.5**	**16.5**	**22.5**
24	Number: 39 Height: 0.54	Number: 9 Height: 1.59	Number: 3 Height: 3.13	Number: 1 Height: 6.10	-
36	Number: 64 Height: 0.55	Number: 15 Height: 1.63	Number: 6 Height: 3.10	Number: 2 Height: 5.76	Number: 1 Height: 9
48	Number: 116 Height: 0.58	Number: 27 Height: 1.73	Number: 11 Height: 3.34	Number: 4 Height: 6.50	Number: 3 Height: 8.1
60	Number: 175 Height: 0.64	Number: 44 Height: 1.83	Number: 19 Height: 3.50	Number: 7 Height: 7.04	Number: 4 Height: 9.90

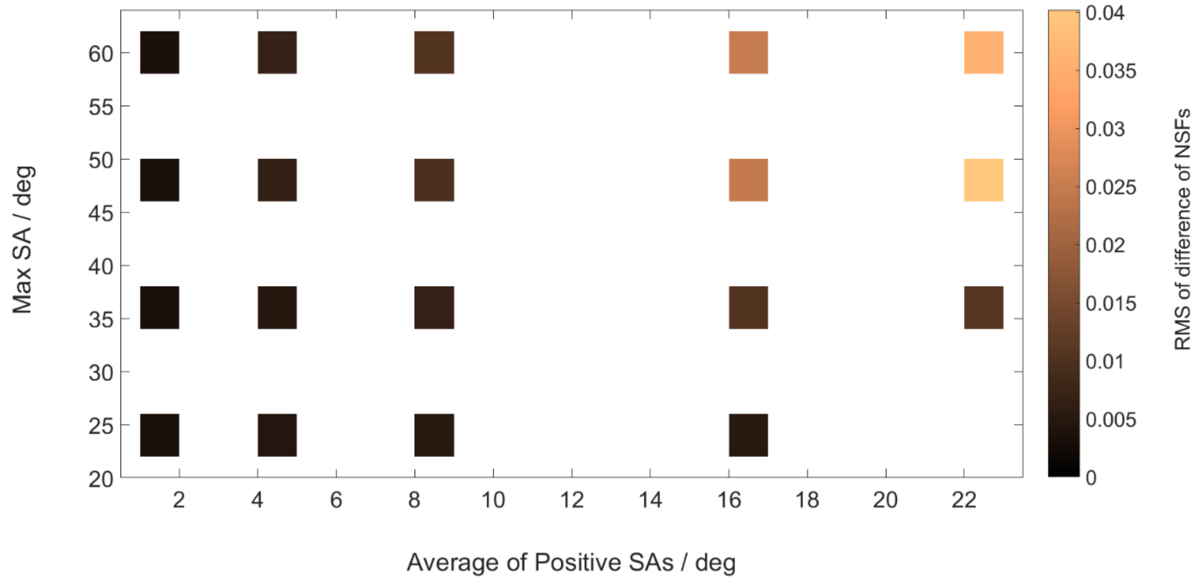

Figure 7. Variations of the RMS of the difference of the NSFs obtained by the BEM and the BK models regarding various combinations of sinusoidal profiles of Table 4 versus changes of the average of positive SAs and maximum SA values of the profile. The length of the profiles was considered 10 times a fixed pitch value (42 μm) for all profiles.

5 Conclusions

In this paper, the validity conditions of the approximate BK model were investigated by comparing the far-field scattering data obtained by the BK model and a rigorous BEM model. The comparison of the BK and the BEM models was quantified by the RMS of the differences of the normalised far-field scattering data.

The scattered fields from a range of various sinusoidal profiles - with different minimum ROC and maximum SA values (using a range of different pitch and height values) - and various combinations of sinusoidal profiles - with different maximum SA and average of positive SAs values (using combinations of a various number of sinusoidal profiles with different heights) - were simulated using the approximate BK model and the rigorous BEM model. Variations of the RMS of the differences of the normalised scattered fields were investigated in terms of the change in the minimum ROC and maximum SA of the sinusoidal profiles, and the maximum SA and average of positive SAs of a combination of the sinusoidal profiles. For profiles with large minimum ROC and low maximum SA, there is a good match between the result obtained by the BK and the BEM models. In this case, the value of the RMS is small ($\lessapprox$ 0.01). Decreasing the minimum ROC and increasing the maximum SA slightly, causes the RMS to increase (0.01 $\lessapprox$ RMS $\lessapprox$ 0.03) due to discrepancies between the results obtained by BK and BEM. By increasing the maximum SA and decreasing the minimum ROC constantly, the difference between the two models will be larger (RMS $\gtrapprox$ 0.03). In order to satisfy the main validity condition of the BK model (RMS $\lessapprox$ 0.02), the minimum ROC of a sinusoidal profile or the average of ROCs of a combination of sinusoidal profiles should be significantly large compared to the wavelength of the incident light (approximately ten times or larger). Although the validity conditions of the BK model depend on the radius of curvature and local angle of incidence, we assumed that the effect of the local incident angle is negligible, since the minimum ROC appears in the minimum of the sinusoidal profile where the local incident angle and the incident angle are the same. It is also shown that the presence of SAs approximately higher than 38° within a sinusoidal profile causes the effect of multiple scattering to appear, which in turn results in the failure of the BK model. However, the BK model can deliver accurate results for a combination of sinusoidal profiles that includes SAs higher than 38° if the average of positive SAs of the profile is lower than 5°.

6 List of Abbreviations

BK	Beckmann-Kirchhoff
BEM	Boundary Element Method
CSI	Coherence Scanning Interferometry
FDTD	Finite Difference Time Domain
FEM	Finite Element Method
NSF	Normalised Scattered Field
PSD	Power Spectral Density
RCWA	Rigorous Coupled-Wave Analysis
RMS	Root-mean-square
ROC	Radius of Curvature
SA	Slope Angle
STF	Surface Trnsfer Funstion
3D	Three-dimensional

Acknowledgements

The authors would like to thank Dr Nikolay Nikolaev (Loughborough University) and Dr Rong Su (Shanghai Institute of Optics and Fine Mechanics) for the use of the BEM and BK codes, respectively, and UKRI Research England Development (RED) Fund for supporting this work via the Midlands Centre for Data-Driven Metrology. This work was supported by the European Metrology Programme for Innovation and Research (EMPIR) project [TracOptic, 20IND07] and the European Union’s Horizon 2020 Research and Innovation programme [DAT4.ZERO, 958363].

References

1. C. J. R. Sheppard, "Scattering and the Spatial Frequency Representation," in *Light Scattering and Nanoscale Surface Roughness*, A. A. Maradudin, Ed., pp. 61-92, Springer US, Boston, MA (2007).
2. P. Beckmann and A. Spizzichino, *The Scattering of Electromagnetic Waves from Rough Surfaces*, Artech House, Norwood, MA (1987).
3. K. G. Larkin, "Efficient nonlinear algorithm for envelope detection in white light interferometry," *J. Opt. Soc. Am. A* **13**(4), 832-843 (1996)
4. P. de Groot and L. Deck, "Surface Profiling by Analysis of White-light Interferograms in the Spatial Frequency Domain," *J. Mod. Opt.* **42**(2), 389-401 (1995)
5. I. Kiselev, E. I. Kiselev, M. Drexel and M. Hauptmannl, "Noise robustness of interferometric surface topography evaluation methods. Correlogram correlation," *Surf. Topogr.: Metrol. Prop.* **5**(4), 045008 (2017)
6. F. Helmli, "Focus Variation Instruments," in *Optical Measurement of Surface Topography*, R. K. Leach, Ed., pp. 131-166, Springer Berlin, Heidelberg (2011).
7. R. Artigas, "Imaging Confocal Microscopy," in *Optical Measurement of Surface Topography*, R. K. Leach, Ed., pp. 237-286, Springer Berlin, Heidelberg (2011).
8. A. Taflove and S. C. Hagness, *Computational Electrodynamics: The Finite-difference Time-domain Method*, Artech House, Boston (2005).
9. J. Elschner, R. Hinder and G. Schmidt, "Finite Element Solution of Conical Diffraction Problems," *Adv. Comput. Math* **16**(2), 139-156 (2002)

10. M. G. Moharam and T. K. Gaylord, "Rigorous coupled-wave analysis of grating diffraction— E-mode polarization and losses," *J. Opt. Soc. Am.* **73**(4), 451-455 (1983)
11. R. F. Harrington, *Field Computation by Moment Methods*, John Wiley & Sons, Inc., New York (1993).
12. T. Pahl, S. Hagemeier, L. Hüser, W. Xie and P. Lehmann, "Two-dimensional modelling of systematic surface height deviations in optical interference microscopy based on rigorous near field calculation," *J. Mod. Opt.* **67**(11), 963-973 (2020)
13. J. Bischoff, T. Pahl, P. Lehmann and E. Manske, *Model-based dimensional optical metrology*, SPIE, (2020).
14. T. Pahl, S. Hagemeier, J. Bischoff, E. Manske and P. Lehmann, "Rigorous 3D modeling of confocal microscopy on 2D surface topographies," *Meas. Sci. Technol.* **32**(9), 094010 (2021)
15. T. Pahl, S. Hagemeier, M. Künne, D. Yang and P. Lehmann, "3D modeling of coherence scanning interferometry on 2D surfaces using FEM," *Opt. Express* **28**(26), 39807-39826 (2020)
16. P. de Groot, X. C. de Lega, J. Liesener and M. Darwin, "Metrology of optically-unresolved features using interferometric surface profiling and RCWA modeling," *Opt. Express* **16**(6), 3970-3975 (2008)
17. L. Fu, K. Frenner and W. Osten, "Rigorous Speckle Simulation Using Surface Integral Equations and Boundary Element Methods," *Fringe 2013: 7th International Workshop on Advanced Optical Imaging and Metrology*, 361-364 (2014)
18. F. S. Salinas, J. L. Lancaster and P. T. Fox, "3D modeling of the total electric field induced by transcranial magnetic stimulation using the boundary element method," *Phys. Med. Biol.* **54**(12), 3631-3647 (2009)
19. M. R. Bai, "Application of BEM (boundary element method)-based acoustic holography to radiation analysis of sound sources with arbitrarily shaped geometries," *J. Acoust. Soc. Am.* **92**(1), 533-549 (1992)

20. G. Manara, A. Monorchio and S. Rosace, "A stable time domain boundary element method for the analysis of electromagnetic scattering and radiation problems," *Eng. Anal. Bound. Elem.* **27**(4), 389-401 (2003)

21. M. Thomas, R. Su, N. Nikolaev, J. Coupland and R. K. Leach, "Modeling of interference microscopy beyond the linear regime," *Opt. Eng.* **59**(3), 034110 (2020)

22. M. Thomas, R. Su, P. de Groot, J. Coupland and R. K. Leach, "Surface measuring coherence scanning interferometry beyond the specular reflection limit," *Opt. Express* **29**(22), 36121-36131 (2021)

23. M. Liu, C. Fai Cheung, N. Senin, S. Wang, R. Su and R. K. Leach, "On-machine surface defect detection using light scattering and deep learning," *J. Opt. Soc. Am. A* **37**(9), B53-B59 (2020)

24. C. J. R. Sheppard, "Imaging of random surfaces and inverse scattering in the Kirchoff approximation," *Waves in Random Media* **8**(1), 53-66 (1998)

25. M. Born and E. Wolf, *Principles of Optics: Electromagnetic Theory of Propagation, Interference and Diffraction of Light*, Cambridge University Press, Cambridge (1999).

26.

27. S. O. Rice, "Reflection of electromagnetic waves from slightly rough surfaces," *Commun. Pure Appl. Math.* **4**(2-3), 351-378 (1951)

28. J. Coupland, R. Mandal, K. Palodhi and R. K. Leach, "Coherence scanning interferometry: linear theory of surface measurement," *Appl. Opt.* **52**(16), 3662-3670 (2013)

29. W. Xie, P. Lehmann, J. Niehues and S. Tereschenko, "Signal modeling in low coherence interference microscopy on example of rectangular grating," *Opt. Express* **24**(13), 14283-14300 (2016)

30. R. Mandal, J. Coupland, R. K. Leach and D. Mansfield, "Coherence scanning interferometry: measurement and correction of three-dimensional transfer and point-spread characteristics," *Appl. Opt.* **53**(8), 1554-1563 (2014)

31. N. Nikolaev, J. Petzing and J. Coupland, "Focus variation microscope: linear theory and surface tilt sensitivity," *Appl. Opt.* **55**(13), 3555-3565 (2016)
32. J. Harvey, A. Krywonos and C. Vernold, "Modified Beckmann-Kirchhoff scattering model for rough surfaces with large incident and scattering angles," *Opt. Eng.* **46**(7), 078002 (2007)
33. S. Schröder, A. Duparré, L. Coriand, A. Tünnermann, D. H. Penalver and J. E. Harvey, "Modeling of light scattering in different regimes of surface roughness," *Opt. Express* **19**(10), 9820-9835 (2011)
34. M. Liu, N. Senin, R. Su and R. K. Leach, "Measurement of laser powder bed fusion surfaces with light scattering and unsupervised machine learning," *Meas. Sci. Technol.* **33**(7), 074006 (2022)
35. E. I. Thorsos and D. R. Jackson, "Studies of scattering theory using numerical methods," *Waves in Random Media* **1**(3), S165-S190 (1991)
36. D. F. McCammon and S. T. McDaniel, "Surface reflection: On the convergence of a series solution to a modified Helmholtz integral equation and the validity of the Kirchhoff approximation," *J. Acoust. Soc. Am.* **79**(1), 64-70 (1986)
37. J. S. Chen and A. Ishimaru, "Numerical simulation of the second-order Kirchhoff approximation from very rough surfaces and a study of backscattering enhancement," *J. Acoust. Soc. Am.* **88**(4), 1846-1850 (1990)
38. H. Hooshmand, M. Liu, R. K. Leach and S. Piano, "Quantifying the validity conditions of the Beckmann-Kirchhoff scattering model," *Proc. SPIE Optical Engineering + Applications*, (2022)
39. I. Simonsen, "Optics of surface disordered systems," *Eur. Phys. J. Spec. Top.* **181**(1), 1-103 (2010)
40. A. A. Maradudin, T. Michel, A. R. McGurn and E. R. Méndez, "Enhanced backscattering of light from a random grating," *Ann. Phys. (N. Y.)* **203**(2), 255-307 (1990)
41. J. J. Sein, "A note on the Ewald-Oseen extinction theorem," *Opt. Commun.* **2**(4), 170-172 (1970)
42. R. Su, J. Coupland, C. Sheppard and R. K. Leach, "Scattering and three-dimensional imaging in surface topography measuring interference microscopy," *J. Opt. Soc. Am. A* **38**(2), A27-A42 (2021)

43. R. Su, Y. Wang, J. Coupland and R. Leach, "On tilt and curvature dependent errors and the calibration of coherence scanning interferometry," *Opt. Express* **25**(4), 3297-3310 (2017)

Caption List

Figure 1 2D BEM scattered field from a sinusoidal profile with 15 μm pitch, 1 μm height and 225 μm length (a) angular distribution of the NSF (unitless), (b) 2D BEM scattered field in the incidence plane.

Figure 2 2D BK scattered field from a sinusoidal profile with 15 μm pitch, 1 μm height and 225 μm length (a) 2D foil model of the surface (generated over the same length, with the display window being trimmed for better visualisation), (b) 2D STF and (c) angular distribution of the NSF (unitless).

Figure 3 Angular distribution of the magnitude of the NSF obtained by the BK and the BEM models for a sinusoidal profile with a minimum ROC of 0.5 μm and maximum SA of 38°.

Figure 4 Variations of the RMS of the differences of the NSFs obtained by the BEM and the BK models for the sinusoidal profiles of Table 1 versus changes in the pitch and height values of the profiles. The length of the profiles was considered ten times the pitch value for each case.

Figure 5 Variations of the RMS of the differences of the NSFs obtained by the BEM and the BK models for the sinusoidal profiles of Table 2 versus changes in the pitch and height values of the profiles. The length of the profiles was 600 μm (including at least ten cycles for each case).

Figure 6 Variations of the RMS of the difference of the NSFs obtained by the BEM and the BK models regarding the sinusoidal profiles of Table 3 versus changes of the minimum ROC and maximum SA values of the profile. The length of the profiles was considered 10 times the pitch value for each case.

Figure 7 Variations of the RMS of the difference of the NSFs obtained by the BEM and the BK models regarding various combinations of sinusoidal profiles of Table 4 versus changes of the average of positive SAs and maximum SA values of the profile. The length of the profiles was considered 10 times a fixed pitch value (42 μm) for all profiles.

Table 1 Specifications of the sinusoidal profiles (in terms of pitch and height values) used to compare the far-field scattering fields obtained by the rigorous BEM and approximate BK models (via the RMS of the differences of the NSFs). Min ROCs are in micrometres.

Table 2 Specification of the sinusoidal profiles (in terms of pitch and height values) used to compare the far-field scattering fields obtained by the rigorous BEM and approximate BK models (via the RMS of the differences of the NSFs). Min ROCs are in micrometres.

Table 3 Specifications of the sinusoidal profiles (in terms of minimum ROC and maximum SA values) used to compare the scattering far-fields obtained by the rigorous BEM and approximate BK models (via the RMS of the differences of the NSFs). Pitches and heights are in micrometres.

Table 4 Specifications of combinations of sinusoidal profiles (in terms of the average of positive SAs and maximum SA values) used to compare the scattering far-fields obtained by the rigorous BEM and approximate BK models (via the RMS of the differences of the NSFs). Heights are in micrometres and the pitch value is fixed at 42 μm for all profiles.